

#### **OPEN ACCESS**

# Charge Transport in the $A_6B_2O_{17}$ (A = Zr, Hf; B = Nb, Ta) Superstructure Series

To cite this article: Tadeusz Miruszewski et al 2024 J. Electrochem. Soc. 171 034503

View the article online for updates and enhancements.

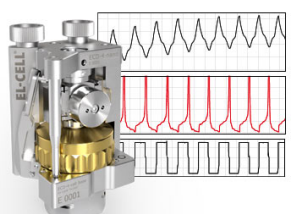
#### You may also like

- The Cosmic-Ray Ionization Rate in the Galactic Disk, as Determined from Observations of Molecular Ions David A. Neufeld and Mark G. Wolfire
- <u>Simulating Hydrodynamics in Cosmology</u> <u>with CRK-HACC</u> Nicholas Frontiere, J. D. Emberson, Michael Buehlmann et al.
- Computational study on intermolecular charge transfer complex of 2,2-bipyridine with picric acid: TD-DFT, NBO and QTAIM analysis

Samia Amirat, Fatiha Madi, Mohamed Bououdina et al.

### Measure the Electrode Expansion in the Nanometer Range.





- Battery Test Cell for Dilatometric Analysis (Expansion of Electrodes)
- Capacitive Displacement Sensor (Range 250 µm, Resolution ≤ 5 nm)
- Detect Thickness Changes of the Individual Electrode or the Full Cell.

www.el-cell.com +49 40 79012-734 sales@el-cell.com









## Charge Transport in the $A_6B_2O_{17}$ (A = Zr, Hf; B = Nb, Ta) Superstructure Series

Tadeusz Miruszewski, <sup>1,z</sup> Aleksandra Mielewczyk-Gryń, <sup>1</sup> Daniel Jaworski, <sup>1</sup> William Foute Rosenberg, <sup>2</sup> Scott J. McCormack, <sup>3,\*</sup> and Maria Gazda <sup>1</sup>

The electrical properties of the entropy stabilized oxides:  $Zr_6Nb_2O_{17}$ ,  $Zr_6Ta_2O_{17}$ ,  $Hf_6Nb_2O_{17}$  and  $Hf_6Ta_2O_{17}$  were characterized. The results and the electrical properties of the products (i.e.  $ZrO_2$ ,  $HfO_2$ ,  $Nb_2O_5$  and  $Ta_2O_5$ ) led us to hypothesize the  $A_6B_2O_{17}$  family is a series of mixed ionic-electronic conductors. Conductivity measurements in varying oxygen partial pressure were performed on  $A_6Nb_2O_{17}$  and  $A_6Ta_2O_{17}$ . The results indicate that electrons are involved in conduction in  $A_6Nb_2O_{17}$  while holes play a role in conduction of  $A_6Ta_2O_{17}$ . Between 900 °C–950 °C, the charge transport in the  $A_6B_2O_{17}$  system increases in Ar atmosphere. A combination of DTA/DSC and in situ high temperature X-ray diffraction was performed to identify a potential mechanism for this increase. In-situ high temperature X-ray diffraction in Ar does not show any phase transformation. Based on this, it is hypothesized that a change in the oxygen sub-lattice is the cause for the shift in high temperature conduction above 900 °C–950 °C. This could be: (i) Nb(Ta)<sup>4+</sup>- oxygen vacancy associate formation/dissociation, (ii) formation of oxygen/oxygen vacancy complexes (iii) ordering/disordering of oxygen vacancies and/or (iv) oxygen-based superstructure commensurate or incommensurate transitions. In-situ high temperature neutron diffraction up to 1050 °C is required to help elucidate the origins of this large increase in conductivity.

© 2024 The Author(s). Published on behalf of The Electrochemical Society by IOP Publishing Limited. This is an open access article distributed under the terms of the Creative Commons Attribution 4.0 License (CC BY, http://creativecommons.org/licenses/by/4.0/), which permits unrestricted reuse of the work in any medium, provided the original work is properly cited. [DOI: 10.1149/1945-7111/ad2d90]

Manuscript submitted October 23, 2023; revised manuscript received January 31, 2024. Published March 7, 2024. This paper is part of the JES Focus Issue on SOFC XVIII: Advances in Solid Oxide Fuel Cell and Electrolysis Cell Technology.

Supplementary material for this article is available online

Mixed oxides among the (ZrO<sub>2</sub>, HfO<sub>2</sub>):(Nb<sub>2</sub>O<sub>5</sub>, Ta<sub>2</sub>O<sub>5</sub>) system have been known for more than 60 years. Since Roth and Coughanour proposed the first ZrO2-Nb2O5 phase diagram and found that 6Zr0<sub>2</sub>·Nb<sub>2</sub>0<sub>5</sub> forms a single-phase orthorhombic structure, several results have been published. So far, mainly structural and thermodynamic properties of  $A_6B_2O_{17}$  (A = Zr, Hf, B = Nb, Ta) have been The orthorhombic unit cell of A<sub>6</sub>B<sub>2</sub>O<sub>17</sub> the compounds is a commensurate superlattice structure built using three distinctive distorted polyhedra, with coordination numbers of six, seven, and eight. Cation-oxygen bond lengths in all four oxides are similar regardless of cation and polyhedron coordination. In Zr<sub>6</sub>Nb<sub>2</sub>O<sub>17</sub>, bond lengths are between 2.086 and 2.177 Å, while in Hf<sub>6</sub>Ta<sub>2</sub>O<sub>17</sub>, Hf<sub>6</sub>Nb<sub>2</sub>O<sub>17</sub> and Zr<sub>6</sub>Ta<sub>2</sub>O<sub>17</sub> bonds range from 2.056 to 2.148 Å, 2.074 to 2.159 Å and 2.077 to 2.161 Å, respectively. Such similarities may be expected to enable the formation of several configurational variants of the structure with different numbers of six, seven and eight coordinated polyhedra. The cation sublattice in these structures is nearly identical, especially since the A and B cations are disordered. For example,  $A_4B_2O_{13}$  and  $A_8B_2O_{21}$  compounds were synthesised.  $^{10,11}$  Others have also identified similar structures such as  $Zr_{x-2}Nb_2O_{2x+1}$ ,  $^{10}$   $Zr_5Nb_2O_{15}$ ,  $^{12}$   $Hf_3Ta_2O_{11}$ ,  $Hf_5Ta_2O_{15}$  and  $Hf_7Ta_2O_{17}$ .  $^{13}$  All these structures are very similar and, in most cases, can only be distinguished by the change in the oxygen sublattice. This variety of structures indicates that the oxygen sublattice within the  $A_6B_2O_{17}$  system may be easily changed.

Voskanyan et al. measured the enthalpy of formation of these  $A_6B_2O_{17}$  compounds and showed that they were positive with respect to their components  $(6AO_2 \text{ and } B_2O_5)$ . This indicating that they are entropy stabilized above a critical temperature (decomposition temperature). A R. Jackson Spurling et al. Deformed in situ X-ray diffraction to observe the formation temperature of the  $A_6B_2O_{17}$  compounds from the their components. Both the measured

decomposition temperature and formation temperature followed similar trends, with  $Hf_6Ta_2O_{17}$  having the highest temperature followed by  $Zr_6Ta_2O_{17}$ ,  $Hf_6Nb_2O_{17}$ ,  $Zr_6Nb_2O_{17}$ .

Until now, only a few functional properties of  $A_6B_2O_{17}$  relevant to engineering applications have been studied. For example,  $Hf_6Ta_2O_{17}$  showed good corrosion resistance as a coating for 33CaO- 9MgO-13AlO<sub>1.5</sub>–45SiO<sub>2</sub>. <sup>16,17</sup> The same material has been also evaluated as possible high-k gate dielectrics for CMOS technology <sup>18</sup> and a sintering crucible in pyroprocessing. <sup>6</sup>  $Zr_6Ta_2O_{17}/8$  YSZ double-ceramic-layer displayed good thermal shock resistance. <sup>19</sup> Additionally, semiconductor heterojunctions of  $Zr_6Nb_2O_{17}$  and  $Nb_2O_5$  or  $ZrO_2$  nanoparticles were studied for their photocatalytic activity. <sup>20</sup> Electrochemical properties relevant to the use of  $Hf_6Ta_2O_{17}$  as supercapacitor electrodes have been reported by Xue et al. <sup>21</sup> To the best of our knowledge, electrical conductivity measurements in the  $A_6B_2O_{17}$  oxides have not been reported.

The search for new materials which exhibit desired electrical properties remains one of the most important goals of modern materials engineering. In recent years, materials with high chemical and/or structural complexity have gained a lot of attention in respect to their electrical conductivity or other interesting phenomena which can be used e.g. in production of electrochemical, thermochemical and many other devices. Therefore, we decided to study this particular system to examine whether it can be of use for future applications. The first step of finding new materials for any application is always to understand the underlining phenomena behind effects like charge transport or structural phase transitions.

To understand the electrical properties of  $A_6B_2O_{17}$ , one should first examine its components:  $ZrO_2$ ,  $HfO_2$ ,  $Nb_2O_5$  and  $Ta_2O_5$ .  $ZrO_2$  undoped and acceptor-doped are ion conductors with some electron/electron-hole contribution to conductivity in a low and high oxygen pressure, respectively. Acceptor-doped  $ZrO_2$  is a widely used solid electrolyte with mobile oxygen vacancies. On the other hand, Moshtaghioun et al. proposed that in the orthorhombic donor-doped  $ZrO_2$ ,  $Zr^{4+}$  cations are the mobile charge carriers. <sup>23</sup> The electrical

<sup>&</sup>lt;sup>1</sup>Institute of Nanotechnology and Materials Engineering, Faculty of Applied Physics and Mathematics, and Advanced Materials Centre, Gdańsk University of Technology, Gdańsk, Poland

<sup>&</sup>lt;sup>2</sup>Department of Chemical Engineering, University of California, Davis, California, 95616, United States of America <sup>3</sup>Department of Materials Science and Engineering, University of California, Davis, California, 95616, United States of America

<sup>\*</sup>Electrochemical Society Member.

<sup>&</sup>lt;sup>z</sup>E-mail: tadeusz.miruszewski1@pg.edu.pl

properties of undoped  $HfO_2$  have recently attracted much attention owing to its application in resistive-switching elements as well as gate dielectrics. The resistive switching in  $HfO_2$  dielectric film occurs as a result of oxide ion diffusion induced by an electric field, leading to the formation of a conductive filament. Ta2O<sub>5</sub> is considered one of the best high-k dielectrics for energy storage capacitors. Its conductivity is predominantly ionic at oxygen partial pressure above  $10^{-4}$  atm and n-type at lower oxygen pressures. Nb2O<sub>5</sub> has been considered a substitute for  $Ta_2O_5$  in solid-state capacitors. It is mainly an electronic conductor with conductivity related to defects, e.g. oxygen vacancies. Thus, since  $ZrO_2$  and  $HfO_2$  are mainly oxide-ion conductors,  $^{28}$   $Ta_2O_5$  is a mixed ionic-electronic conductor and  $Nb_2O_5$  is mainly an electronic conductor, it is expected that compounds in the  $A_6B_2O_{17}$  series will be mixed ionic-electronic conductors.

In this work, we present and discuss the electrical properties of  $Zr_6Nb_2O_{17},\ Hf_6Nb_2O_{17},\ Zr_6Ta_2O_{17}$  and  $Hf_6Ta_2O_{17}$  (The  $A_6B_2O_{17}$  series) up to 1050 °C in synthetic air (20%  $O_2/80\%$   $N_2)$  and Ar, along with thermogravimetric analysis and in situ X-ray diffraction in an attempt to elucidate mechanisms. For the first time complex charge transport properties within the  $A_6B_2O_{17}$  system have been studied, providing insight into how structural complexity can greatly influence electrical transport properties.

#### **Experimental**

A<sub>6</sub>B<sub>2</sub>O<sub>17</sub> compounds were synthesized using the Steric Entrapment Method.  $^{29,30}$  ACl<sub>4</sub>, where A = Hf (99.9%, Sigma Aldrich), Zr (99.99%, Sigma Aldrich), was dissolved in DI water. BCl<sub>5</sub>, where B = Ta (99.9%, Sigma Aldrich, Nb (99.9%, Sigma Aldrich), was dissolved in HPLC Grade Isopropyl alcohol. Solutions of ACl<sub>4</sub> and BCl<sub>5</sub> were then mixed and allowed to homogenize. Ethylene Glycol (99.8%, Sigma Aldrich) was added in a 4:1 cation to OH ratio. The mixture was heated and stirred on a hotplate until reduced to a clear gel. The gel was dried in a vented oven overnight at 400 °C. Dried product was then ground in an Yttria Stabilized (YSZ) mortar and pestle and calcined in a lidded YSZ crucible at 1050 °C for 12 h. The product was then pressed into a 20 mm pellet at 155 MPa using an MTI cold isostatic hydraulic press. The pellet was then annealed at 1300 °C for 12 h in a lidded YSZ crucible with a heating and cooling rate of 5 °C min<sup>-1</sup>. Phase identification of synthesized powders was determined using a Bruker D-8 X-ray Diffractometer (Copper K- $\alpha$ ,  $\lambda = 1.5406 \text{ Å}$  ). Chemical purity was checked using a Rigaku X-ray Fluorescence spectrometer using Boric Acid substrate shells (5 mm, Vprep Corp). To prepare dense pellets, the powders were pressed using 300 MPa and sintered at 1500 °C for two hours. The densities of pellets were determined using the Archimedes law with kerosene as liquid medium. As for the Zr<sub>6</sub>Nb<sub>2</sub>O<sub>17</sub> and Hf<sub>6</sub>Nb<sub>2</sub>O<sub>17</sub> pellets the relative density was 97% and 86%, respectively, while that of Zr<sub>6</sub>Ta<sub>2</sub>O<sub>17</sub> and Hf<sub>6</sub>Ta<sub>2</sub>O<sub>17</sub> is lower, between 67% and 69%. It is also worth mentioning that the colour of the samples after sintering slightly differed. The samples with Ta in the structure were white while the ones with Nb were offwhite. The cause behind that can be quite complex, from the differences in cation chemistry to colour centre formation.

The microstructure of the samples was examined using the FEI Quanta FEG 250 scanning microscope (SEM). The micrographs were obtained based on the signal from secondary electrons (SE), which was recorded using Everhart-Thornley Detector (ETD). The imagining was carried out in high-vacuum mode with an acceleration voltage of 30 kV. For better quality of the images, all samples were gold coated.

Temperature dependence of conductivity was studied with electrochemical impedance spectroscopy (EIS) in the temperature range of 600-1050 °C in synthetic air (20% oxygen, 80% nitrogen) and argon atmospheres. Platinum electrodes were applied to cylindrical pellets with a diameter of  $\sim 1$  cm using Pt-paste (ESL 5542) and heated at a temperature of 930 °C for 3 h. Thus, the electrical studies were performed in the *Pt/sample/Pt* cells prepared

in this way. It is worth noting that all electrical measurements for a specific chemical composition were performed on one prepared cell. EIS measurements were performed using Gamry Reference 3000 potentiostat in the frequency range from 1 Hz to 1 MHz with signal amplitude (100 mV–1 V) depending on sample resistance. Additionally, the oxygen partial pressure dependence of conductivity was studied in pure oxygen (pO $_2=1\,\mathrm{atm}$ ), pure nitrogen (pO $_2=10^{-6}\,\mathrm{atm}$ ) and their mixtures. The frequency range and signal amplitude were adjusted according to resistance level.

The total resistances and capacitances obtained from the analysis of the impedance spectra allowed for the determination of conductivities using Eq. 1.

$$\sigma_{tot} = \frac{1}{R_{tot}} \cdot \frac{l}{S} \tag{1}$$

where  $R_{tot}$  is total resistance,  $\sigma_{tot}$ —total electrical conductivity, l - the thickness of the sample and S - the surface area of the electrodes. The Bruggeman asymmetric model was applied for porosity correction of the total electrical conductivity.  $^{31}$ 

To study shifts in oxygen stoichiometry, thermogravimetric analysis (TGA) was carried out. Measurements in air were undertaken using Netzsch Tarsus thermobalance at a temperature range of RT-900 °C. Measurements in argon were performed using Netzsch STA 449 at a temperature range of RT-1100 °C. In both measurements, the temperature was increased at a rate of 5 °C min<sup>-1</sup> with a purge/protective gas flow rate of 20/40 ml min<sup>-1</sup>. Blanks were performed before each measurement to account for the buoyancy effect.

To verify phase composition between  $25-1050\,^{\circ}\mathrm{C}$  in argon, in situ high-temperature diffractometry was performed using a Philips X'pert Pro MPD system equipped with an Anthon Paar HTK1200 camera.

#### **Results and Discussion**

In Fig. 1, the cross-section images of the microstructure of all studied samples are presented.

It can be seen that all the ceramics exhibit a grain size between  $\sim\!1\!-\!4~\mu m$ . The grains of the samples with Nb (Figs. 1a and 1c) are larger than those in the samples containing Ta. Moreover, grains in  $Zr_6\mathrm{Nb}_2\mathrm{O}_{17}$  and  $Hf_6\mathrm{Nb}_2\mathrm{O}_{17}$  have different shapes from the other ceramics. The samples containing niobium have lower porosity than samples with tantalum. This observation is consistent with the results obtained from density measurements.

The results of EIS experiments obtained in an Ar atmosphere were used to produce Nyquist plots of Zr<sub>6</sub>Nb<sub>2</sub>O<sub>17</sub>, Zr<sub>6</sub>Ta<sub>2</sub>O<sub>17</sub>, Hf<sub>6</sub>Nb<sub>2</sub>O<sub>17</sub>, Hf<sub>6</sub>Ta<sub>2</sub>O<sub>17</sub> densified pellets. Figure 2 shows Zr<sub>6</sub>Nb<sub>2</sub>O<sub>17</sub> along with the circuits used to model the impedance. The Nyquist plots obtained for Hf<sub>6</sub>Ta<sub>2</sub>O<sub>17</sub>, Zr<sub>6</sub>Ta<sub>2</sub>O<sub>17</sub> and Hf<sub>6</sub>Nb<sub>2</sub>O<sub>17</sub> are shown in Figs. S1-S3 in the supplementary information file. In the low-temperature range (Fig. 2a) three semicircles which are seen in the plot were represented by the  $R_g$ ,  $R_{gb}$  and  $R_e$  resistors paired with the  $CPE_g$ ,  $CPE_{gb}$  and  $CPE_e$  constant phase elements, respectively. The g, gb and e subscripts signify grain, grain boundary and electrode components. The semicircle of grain impedance  $(R_g \text{ and } CPE_g)$  is observed in the high-frequency range while the low-frequency ones correspond to grain boundaries  $(R_{eb}$  and  $CPE_{eb})$  and the electrode  $(R_e$  and  $CPE_e)$ . In the case of the studied samples, we did not observe an electrical response from the grains in the high-temperature range (see Fig. 2b), hence the model simply uses one  $R_{\varrho}$  resistor instead of  $R_{\varrho}$  and  $CPE_{\varrho}$ .

Figure 3 depicts the temperature dependence of the total conductivity of the  $A_6B_2O_{17}$  compounds between 600 and 1050 °C in air and argon atmospheres, as measured by EIS. In the  $A_6B_2O_{17}$  systems, the total conductivity increases with temperature, indicating thermally activated charge carrier transport. In an Argon atmosphere, a rapid increase in conductivity above  $\sim 950$  °C is observed. The total

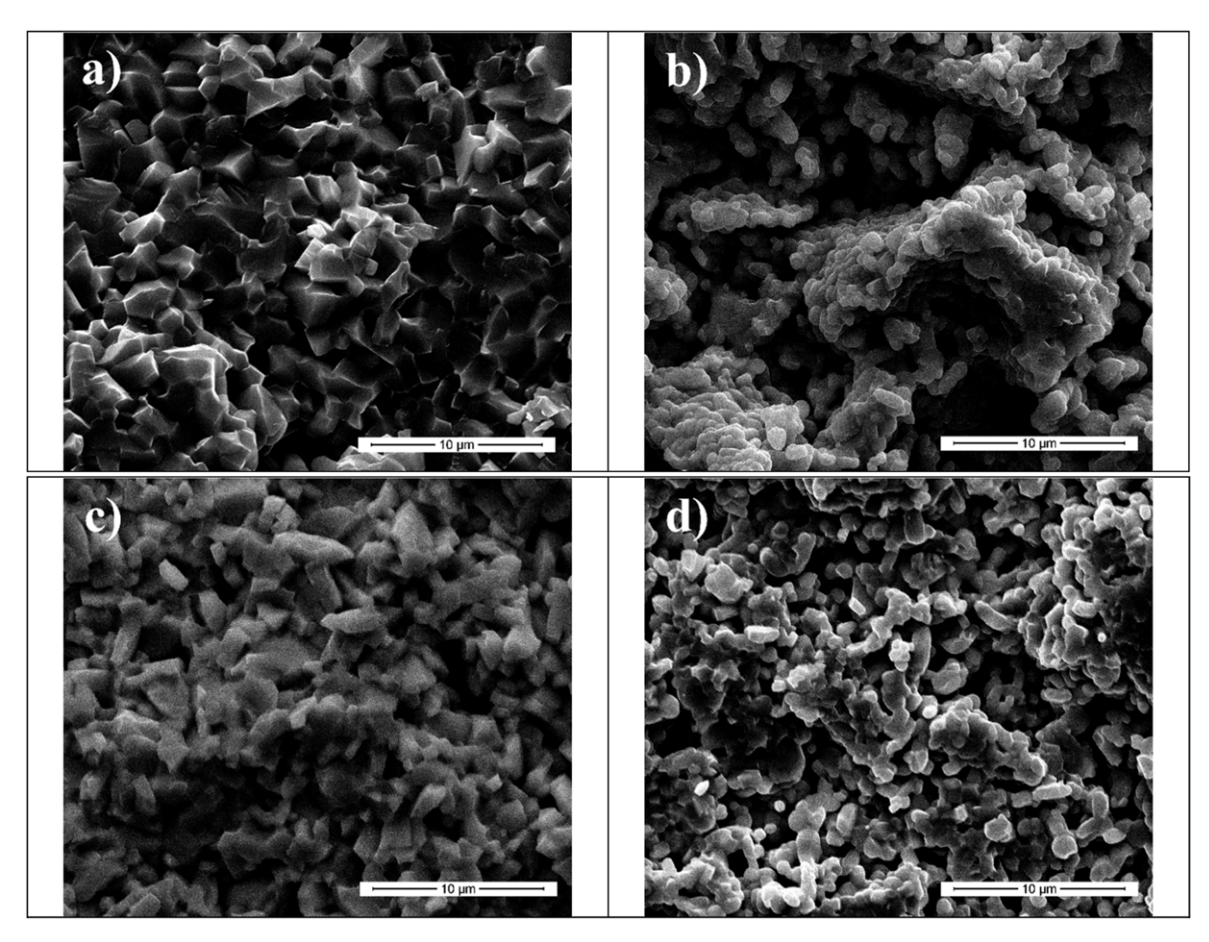


Figure 1. SEM cross-section images of (a)  $Zr_6Nb_2O_{17}$ , (b)  $Zr_6Ta_2O_{17}$ , (c)  $Hf_6Nb_2O_{17}$  and (d)  $Hf_6Ta_2O_{17}$ .

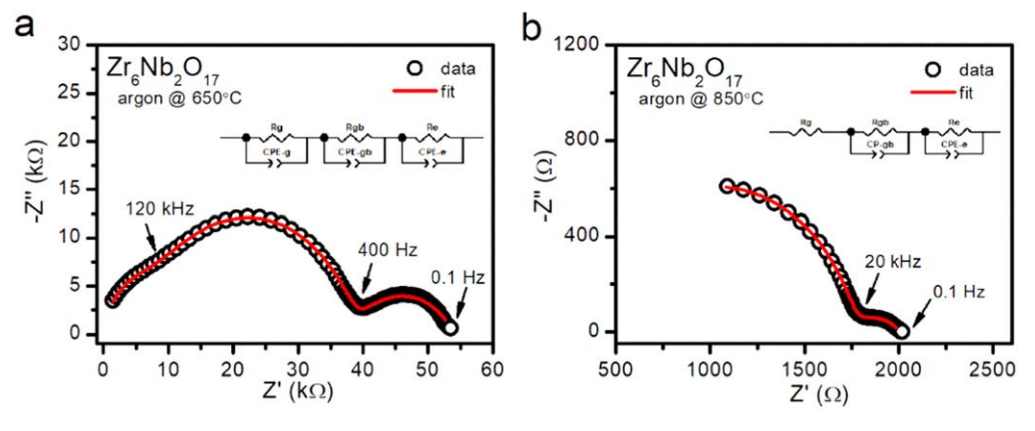


Figure 2. The impedance Nyquist plots of  $Zr_6Nb_2O_{17}$  in an argon atmosphere at 650 °C (a) and 850 °C (b). The plots for  $Zr_6Ta_2O_{17}$ ,  $Hf_6Nb_2O_{17}$  and  $Hf_6Ta_2O_{17}$  are shown in the supplementary materials (Figs. S1–S3).

conductivity in argon atmosphere at 1050 °C in  $Hf_6Ta_2O_{17}$ ,  $Zr_6Nb_2O_{17}$ ,  $Hf_6Nb_2O_{17}$  and  $Zr_6Ta_2O_{17}$  and was 13, 22, 36 and 49 times higher than that in air, respectively. For thermally activated transport in oxides, several transport mechanisms may be responsible e.g. ionic conduction, polaron hopping or electron/hole band transport. The slope of the  $\log \sigma(1/T)$  plots shown in Fig. 3 were used to determine the apparent activation energies for charge transport and are tabulated in Table I. These apparent activation energies are between 1 and 1.8 eV. The rapid increase in conductivity in argon at high temperatures which was described by "E<sub>a</sub>" between 2 and 6 eV is a very interesting phenomenon.

The key electrical transport trends as measured from EIS for the  $A_6B_2O_{17}$  compounds can be summarized as follows:

- (1) The conductivity of  $A_6Nb_2O_{17}$  is higher than that of  $A_6Ta_2O_{17}$ ;
- 2) The conductivity in air of  $Hf_6B_2O_{17}$  is higher than that of  $Zr_6B_2O_{17}$ . The same relation is observed for  $A_6Nb_2O_{17}$  in argon whereas the conductivity of  $Zr_6Ta_2O_{17}$  in argon is slightly higher than that of  $Hf_6Ta_2O_{17}$ .
- (3) In A<sub>6</sub>Nb<sub>2</sub>O<sub>17</sub> apparent activation energy of conduction in air at lower temperatures is higher than at higher temperatures, whereas in A<sub>6</sub>Ta<sub>2</sub>O<sub>17</sub> it is either lower or the same.

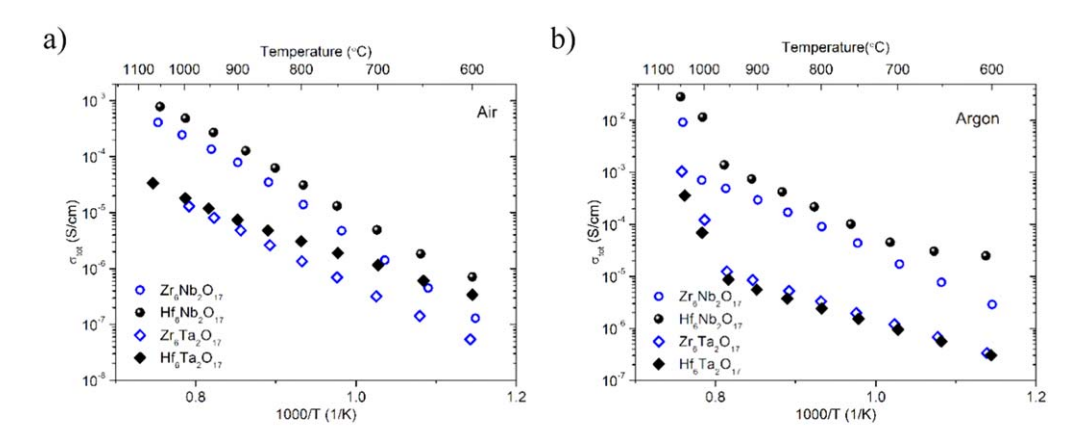


Figure 3. Temperature dependence of the total conductivity of A<sub>6</sub>B<sub>2</sub>O<sub>17</sub> between 600 and 1000 °C in air (a) and argon atmospheres (b).

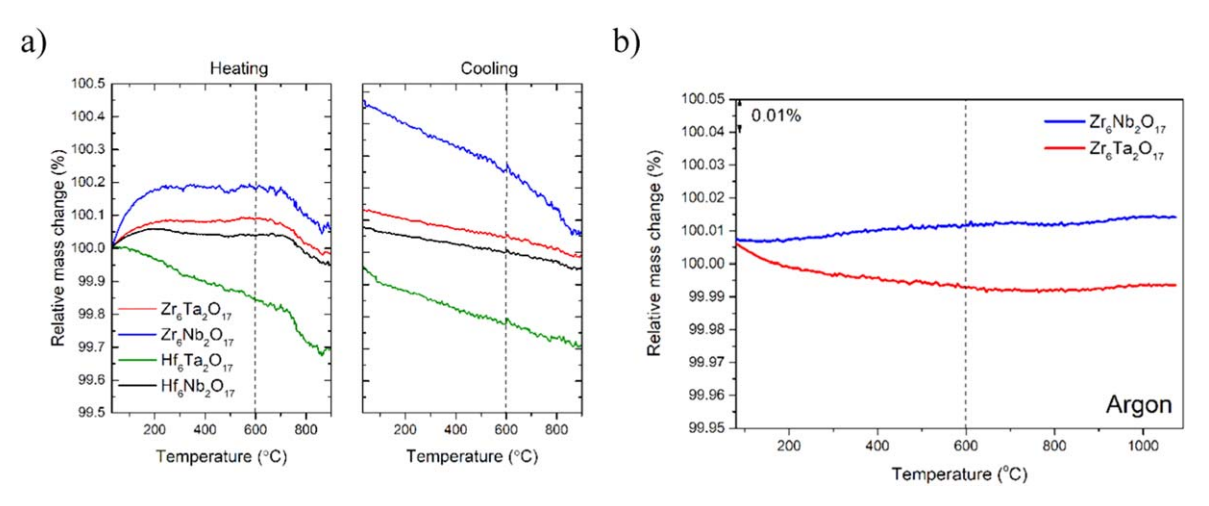


Figure 4. Thermogravimetric analysis of  $Hf_6Ta_2O_{17}$ ,  $Hf_6Nb_2O_{17}$  and  $Zr_6Ta_2O_{17}$  in synthetic air (a) and of  $Zr_6Nb_2O_{17}$  and  $Zr_6Ta_2O_{17}$  oxides in argon (b).

Table I. Apparent activation energies and	values of total conductivity in different conditions.

Sample	Atmosphere	Low temperatures		High temperatures	
		E <sub>a</sub> (eV)	σ(700 °C) 10 <sup>-6</sup> Scm <sup>-1</sup>	E <sub>a</sub> (eV)	σ(1050 °C) 10 <sup>-6</sup> Scm <sup>-1</sup>
Hf <sub>6</sub> Nb <sub>2</sub> O <sub>17</sub>	Air	1.77	4.9	1.48	790
	Argon	1.55	45	$2.9^{a)}$	28300
	•	(10)			
$\mathrm{Zr_6Nb_2O_{17}}$	Air	1.96	1.4	1.54	410
	Argon	1.46	17	1.9 <sup>a)</sup>	9200
$\mathrm{Hf_6Ta_2O_{17}}$	Air	0.98	1.15	1.34	28
	Argon	0.95	0.95	$6.0^{a)}$	360
$Zr_6Ta_2O_{17}$	Air	1.44	0.32	1.44	24 <sup>b)</sup>
	Argon	1.04	1.2	1.8 <sup>a)</sup>	1040

a)  $E_a$  values in the high-temperature range in the argon atmosphere should not be treated as activation energies of conduction. b) The conductivity of  $Zr_6Ta_2O_{17}$  at 1050 °C in the air was approximated based on the temperature dependence measured up to 1000 °C.

(4) The total conductivity of  $Zr_6Nb_2O_{17}$ ,  $Hf_6Nb_2O_{17}$  and  $Zr_6Ta_2O_{17}$  below 900 °C in air is lower than that in argon, whereas the conductivity of  $Hf_6Ta_2O_{17}$  is higher in air.

The difference between the conductivities of  $A_6 Nb_2 O_{17}$  and  $A_6 Ta_2 O_{17}$  is between approximately 0.5 and 1 order of magnitude. The influence of the A-cation, i.e. Zr and Hf, on the total conductivity of either  $A_6 Nb_2 O_{17}$  or  $A_6 Ta_2 O_{17}$  is weaker. Hf and Zr have almost the same ionic radii and ionization energies so all redox and defect-related

properties are quite similar.  $^{32}$  Different ion masses may be expected to influence properties related to vibrations. E.g. activation energy of thermally activated phenomena may be expected to be different. It may be one of the reasons for the lower apparent activation energy of total conductivity in air for  $Hf_6B_2O_{17}$  in comparison to that of  $Zr_6B_2O_{17}$ . With a much higher atomic mass of Hf in comparison to Zr, one may assume that the frequencies of phonons related to the  $Zr_6B_2O_{17}$  compounds. As was mentioned earlier,

 $Hf_6Ta_2O_{17}$  has the highest decomposition temperature followed by  $Zr_6Ta_2O_{17}, Hf_6Nb_2O_{17}$  and  $Zr_6Nb_2O_{17}.$  This tendency agrees well with the changes in the average cation electronegativity which for  $Hf_6Ta_2O_{17}, Zr_6Ta_2O_{17}, Hf_6Nb_2O_{17}$  and  $Zr_6Nb_2O_{17}$  are 1.255, 1.247, 1.230 and 1.222 in Allred-Rochov scale, respectively. Thus, one can say that the  $A_6Ta_2O_{17}$  are less stable and form more covalent cation-oxide bonds than the  $A_6Nb_2O_{17}.$  These differences are not large but may be one of the reasons for differences in electrical properties.

To understand the electrical properties of A<sub>6</sub>B<sub>2</sub>O<sub>17</sub>, one should examine its components: ZrO<sub>2</sub>, HfO<sub>2</sub> and Nb<sub>2</sub>O<sub>5</sub> and Ta<sub>2</sub>O<sub>5</sub>. As it was mentioned earlier, ZrO2 and HfO2 are mainly oxide-ion conductors, <sup>28</sup> Ta<sub>2</sub>O<sub>5</sub> is a mixed ionic-electronic conductor <sup>26</sup> whereas Nb<sub>2</sub>O<sub>5</sub> is mainly an electronic conductor.<sup>27</sup> Thus, it is expected that the A<sub>6</sub>B<sub>2</sub>O<sub>17</sub> series will be mixed ionic-electronic conductors. The defects which predominantly form in ZrO2 and HfO2, and determine their conductivity are oxygen vacancies. Also, Nb<sub>2</sub>O<sub>5</sub> and Ta<sub>2</sub>O<sub>5</sub> tend to be oxygen-deficient. Oxygen deficiency may be related to the presence of either oxygen vacancies compensated by the reduction of the Nb/Ta valence state from 5+ to 4+, or cation interstitial defects. The latter is considered less probable<sup>33</sup> though cannot be neglected. For example, TiO<sub>2</sub> is an oxygen-deficient oxide with a multivalent metal, similar to the A<sub>6</sub>B<sub>2</sub>O<sub>17</sub> compounds. When TiO<sub>2</sub> is exposed to intermediate oxygen partial pressures, oxygen vacancies tend to dominate, while at low oxygen partial pressures, titanium interstitials tend to dominate.<sup>34</sup> Thus, mixed defects should be taken into consideration for the A<sub>6</sub>B<sub>2</sub>O<sub>17</sub> structure. Moreover, Nb<sub>2</sub>O<sub>5</sub> and Ta<sub>2</sub>O<sub>5</sub> inevitably contain acceptor impurities which further promote the formation of oxygen vacancies. Xue et al. found that annealing Hf<sub>6</sub>Ta<sub>2</sub>O<sub>17</sub> in reducing atmospheres leads to an increase in oxygen vacancy concentration. <sup>21</sup> They also found that in the process of reduction, the tantalum oxidation state decreased while the unit cell parameters and volume did not change as expected.

The interesting point, in the chase of zirconium-based systems, was mentioned by Moshtaghioun et al. in their study on tantalum doped orthorhombic zirconia. They suggest the possibility of zirconium ion diffusion, with substantially low activation energy, in ceramics. This can possibility be a minor effect in zirconium containing system, however, we are more inclined, based on the activation energy values, to attribute the conductivity to oxygen than cation diffusion. Thus, we propose that the main defects which form in Hf<sub>6</sub>Ta<sub>2</sub>O<sub>17</sub>, Zr<sub>6</sub>Nb<sub>2</sub>O<sub>17</sub>, Hf<sub>6</sub>Nb<sub>2</sub>O<sub>17</sub> and Zr<sub>6</sub>Ta<sub>2</sub>O<sub>17</sub> are oxygen vacancies whose charge is compensated by the reduction of Nb and Ta, as described by reaction (2).

$$O_O^X \leftrightarrow V_O^{\bullet \bullet} + 2Nb'(Ta)'_{Nb(Ta)} + \frac{1}{2}O_2$$
 [2]

Where  $O_O^X$  is the lattice oxygen ion,  $V_O^{\bullet \bullet}$  - doubly ionized oxygen vacancy and  $2Nb'(Ta)'_{Nb(Ta)}-4+$  Nb or Ta ion in its lattice position. This is consistent with the previously stated expectation that the  $A_6B_2O_{17}$  series are mixed conductors with mobile electrons/holes and oxide ions.

To gain more information regarding the possible reduction and oxidation of oxides in the  $A_6B_2O_{17}$  series and the influence of the atmosphere on the structural and electrical properties, thermogravimetric analysis and in situ high temperature X-ray powder diffraction (XRPD) were performed. The results of the thermogravimetric analysis in air and argon atmospheres are shown in Fig. 4, and the high temperature XRPD in Fig. 5. The mass of the synthesized  $A_6B_2O_{17}$  powders while heated in air, increases with increasing temperature, until saturation, and then above approximately 700 °C decreases. Of the four compounds, only  $Hf_6Ta_2O_{17}$  appears to be reduced in the studied temperature range, the other compositions' mass after increase during thermal oxidation goes back to the initial mass value at 900 °C. Subsequent heating in the air leads to reoxidation and the mass increases above the initial value.

The change in the mass of  $A_6B_2O_{17}$  oxide powders in air demonstrates that the oxygen stoichiometry can change. However, the

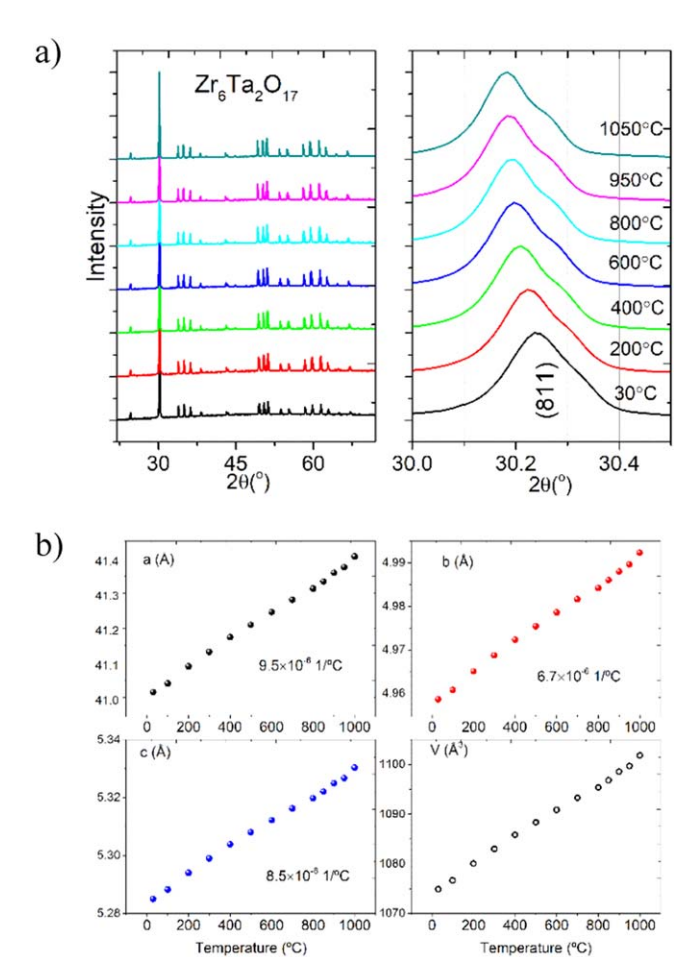


**Figure 5.** X-ray diffractograms of  $Zr_6Ta_2O_{17}$  at different temperatures below 1050 °C in argon and expanded region of  $2\theta \sim 30^\circ$  showing the main, (811), reflection (a), and temperature dependence of unit cell parameters and volume (b).

mass change in Ar is comparatively small. A key observation is that within the temperature range of 900–950 °C, where the dramatic increase in conductivity was observed, the mass change is nearly constant.

In-situ high temperature X-ray diffraction of  $Zr_6Ta_2O_{17}$  was performed from room temperature to 1050 °C in argon (Fig. 5). Over the temperatures studied, the X-ray diffraction patterns remain the same while the unit cell parameters increase nearly linearly with temperature. Since the TGA highlights that the conductivity increase is not directly related to reduction or change in oxygen non-stoichiometry and the HT-XRD of  $Zr_6Ta_2O_{17}$  from room temperature up to  $1050\,^{\circ}\text{C}$  in argon indicate no observable change in structure, so the rapid conductivity increase must be driven by a different mechanism.

Thus, the mechanism related to the change in observed charge transport at elevated temperature in Ar may be a subtle structural change, such as: (i)  $Nb(Ta)^{4+}$ - oxygen vacancy associate formation/dissociation, (ii) formation of oxygen/oxygen vacancy complexes (iii) ordering/disordering of oxygen vacancies and/or (iv) oxygen-based superstructure commensurate or incommensurate transitions, which cannot be detected by XRD. We believe such changes in the oxygen sublattice structure are responsible for the observed increase in total conductivity at high temperatures in argon. In-situ high-temperature neutron diffraction studies are required to probe the oxygen sublattice in the  $A_6B_2O_{17}$  series in argon and air above 950 °C to help elucidate possible mechanisms.

EIS measurements were also conducted on  $Hf_6Nb_2O_{17}$  and  $Hf_6Ta_2O_{17}$  below 900 °C to determine the effect of oxygen partial pressure. The results are displayed in Fig. 6.

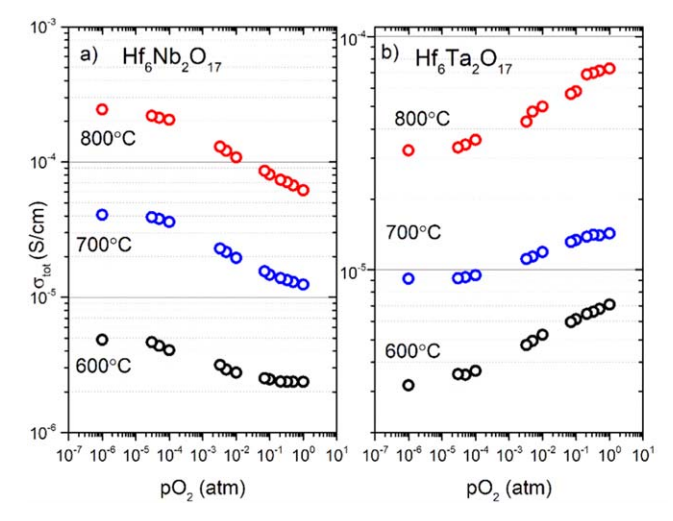


**Figure 6.** Total conductivity of (a)  $Hf_6Nb_2O_{17}$  and (b)  $Hf_6Ta_2O_{17}$  at 600, 700 and 800 °C as a function of oxygen partial pressure.

The total conductivity is not constant in a wide range of the oxygen partial pressures. In agreement with the results shown in Fig. 3 the conductivity of Hf<sub>6</sub>Nb<sub>2</sub>O<sub>17</sub> increases whereas that of Hf<sub>6</sub>Ta<sub>2</sub>O<sub>17</sub> decreases with decreasing oxygen partial pressure. Apart from oxide ions, this indicates that the charge carriers that play an important role in conduction are electrons in A<sub>6</sub>Nb<sub>2</sub>O<sub>17</sub> and holes in A<sub>6</sub>Ta<sub>2</sub>O<sub>17</sub>. The observed dependence of conductivity on the pO<sub>2</sub>  $(\sigma \sim (pO_2)^{\frac{1}{n}}$  where  $\frac{1}{n} \approx -0.117$  at 800 °C) for Hf<sub>6</sub>Nb<sub>2</sub>O<sub>17</sub> does not follow known simple models. Typically,  $n = -6 \left(\frac{1}{n} \approx -0.167\right)$  is expected in low oxygen partial pressures if the oxygen vacancies are charge compensated by electrons.<sup>34</sup> Thus, the charge carrier which dominates conduction cannot be unambiguously stated. These types of deviations have been observed in other systems. For example,  $ZrO_2$ , which is considered a model system, typically has a  $(pO_2)^{1/6}$ and  $(pO_2)^{-1/6}$  dependence which dominates respectively at high and low oxygen partial pressures. However, other experiments by Kim et al. found  $\sim$ 0.17 and -0.13 exponents at high and low oxygen partial pressures, respectively.<sup>35</sup> The only conditions in which the conductivity is quasi-independent of the oxygen partial pressure are below  $10^{-5}$  atm at some temperatures. This supports the hypothesis that the A<sub>6</sub>B<sub>2</sub>O<sub>17</sub> oxides in most of the conditions studied in this work are mixed ionic-electronic conductors. An unusual oxygen partial pressure dependence of conductivity suggests more complex transport properties. Again, these results suggest that the observed conductivity is driven by the oxygen sublattice. The proposed earlier processes, i.e. oxygen vacancy associate formation/dissociation, formation of oxygen/oxygen vacancy complexes, ordering/disordering of oxygen vacancies and/or oxygen-based superstructure commensurate or incommensurate transitions, may occur at different temperatures and/or oxygen partial pressures. These most likely influence both the concentration and mobility of charge carriers. Therefore, although the A<sub>6</sub>B<sub>2</sub>O<sub>17</sub> structures are similar to one another, subtle differences in structural, thermal, and electronic structure may alter electrical properties. What is more, these differences most likely affect both ionic and electronic-type conductivities.

The structural features important for oxide-ion conductivity are the number and energy of available positions between which ions may jump, the energy barrier height between them, defect association energy etc. We assume the vacancy mechanism, typical of  $ZrO_2$  and  $HfO_2$ , is also most probable in oxygen-deficient  $A_6B_2O_{17}$ . For vacancy-type ionic conductivity, a random distribution of oxygen vacancies around equivalent sites is the most favourable

environment. Structural studies show two features important for ionic conduction: (i) the cations are 6-, 7- and 8-fold coordinated and (ii) there are 7 different positions for oxygen in the unit cell of  $A_6B_2O_{17}$ . The possibility of different coordination numbers of cations should favour oxide ion mobility whereas the presence of inequivalent sites is expected to hinder migration, increasing its activation energy. The structural properties of the  $A_6B_2O_{17}$  series are surprisingly similar, most significant difference relevant to ion conduction is the much higher temperature factor for oxygen in  $Hf_6Ta_2O_{17}$  compared to the other three oxides. It may indicate higher mobility of the oxide ions and could be one of the reasons why the apparent activation energy of conduction in  $Hf_6Ta_2O_{17}$  is the lowest. Further studies, in particular theoretical calculations, are necessary to find the most probable migration path of the oxygen vacancies.

To discuss electronic conductivity, the electronic structure of the A<sub>6</sub>B<sub>2</sub>O<sub>17</sub> family should be known. Kleger and Meunier with the DFT method for Hf<sub>6</sub>Ta<sub>2</sub>O<sub>17</sub> found an indirect band gap of 2.67 eV<sup>36</sup> whereas Bai et al. experimentally determined the bandgap of Zr<sub>6</sub>Nb<sub>2</sub>O<sub>17</sub> as 2.78 eV, also indirect.<sup>20</sup> The bandgap of 2.67 eV would mean that Hf<sub>6</sub>Ta<sub>2</sub>O<sub>17</sub> absorbs blue and violet light which is not observed. All oxides are white (A<sub>6</sub>Ta<sub>2</sub>O<sub>17</sub> are even whiter than A<sub>6</sub>Nb<sub>2</sub>O<sub>17</sub> which in the form of pellets are slightly greyish) and knowing that DFT usually underestimates the bandgap value, we may assume the bandgap of all studied oxides is at least 2.8 eV. This could explain the apparent activation energy of the conduction  $E_a = \frac{1}{2}E_g$  of reduced Hf<sub>6</sub>Nb<sub>2</sub>O<sub>17</sub> and Zr<sub>6</sub>Nb<sub>2</sub>O<sub>17</sub> (in air at high temperatures and argon at low temperatures) and Zr<sub>6</sub>Ta<sub>2</sub>O<sub>17</sub> in air. On the other hand, the reduced Zr<sub>6</sub>Ta<sub>2</sub>O<sub>17</sub> and Hf<sub>6</sub>Ta<sub>2</sub>O<sub>17</sub> show lower activation energy of conduction than that corresponding to the bandgap. It is possible that in A<sub>6</sub>Ta<sub>2</sub>O<sub>17</sub> the reduction causes the bandgap to narrow or introduces a sufficiently high number of the states in the bandgap.

#### Conclusions

In the  $A_6B_2O_{17}$  (where A=Zr, Hf and B=Nb, Ta) series, the charge carrier transport was determined by thermally activated processes. We proposed that the defects which form in  $Hf_6Ta_2O_{17}$ ,  $Zr_6Nb_2O_{17}$ ,  $Hf_6Nb_2O_{17}$  and  $Zr_6Ta_2O_{17}$  are oxygen vacancies whose charge is compensated by the reduction of niobium and tantalum.

The  $A_6B_2O_{17}$  series are mixed electronic-ionic conductors with oxide ions and electron or electron-hole mobile charge carriers. Subtle differences in electronic, thermal, and structural properties were discussed as possible reasons for different electrical properties. Electrons are expected to play a large role in  $A_6Nb_2O_{17}$  conduction, while holes are expected to play a large role in  $A_6Ta_2O_{17}$  conduction.

A rapid increase in conductivity was observed in the entire  $A_6B_2O_{17}$  series in Ar at 900–950 °C. This increase in conductivity was not due to oxygen vacancy population as determined by TGA and/or structural transformation as determined by in situ X-ray diffraction. Because of this, the increase in conductivity is expected be a subtle structural change in the oxygen sublattice which cannot be detected by X-ray diffraction. These could include: (i) Nb(Ta)<sup>4+</sup>oxygen vacancy associate formation/dissociation, (ii) formation of oxygen/oxygen vacancy complexes (iii) ordering/disordering of oxygen vacancies and/or (iv) oxygen-based superstructure commensurate or incommensurate transitions which may occur at different temperatures and/or oxygen partial pressures. This most likely influences both the concentration but also the mobility of charge carriers. Therefore, although the A<sub>6</sub>B<sub>2</sub>O<sub>17</sub> structures are similar to one another, subtle differences in atomic, thermal, and electronic structure may alter electrical properties. What is more, these differences most likely affect both ionic and electronic-type conductivities. In-situ high-temperature neutron diffraction studies would give more insight into variations in the oxygen sub-lattice

and could lead to an enhanced mechanistic understanding of the observed results.

#### Acknowledgments

The research was financially supported by the National Science Centre (NCN), Poland within the project 2019/35/B/ST5/00888 and by the National Science Foundation (NSF) in the Directorate for Mathematical and Physical Sciences (MPS), under the Division of Materials Research (DMR), in the Ceramic (CER) program, award number: 2047084.

#### **Supporting Information**

The publication includes supporting information that presents additional Nyquist plots for impedance studies. These results constitute an attachment to this research work.

#### **ORCID**

Tadeusz Miruszewski https://orcid.org/0000-0002-9829-9738 Daniel Jaworski https://orcid.org/0000-0001-5791-6413

#### References

- R. S. Roth and L. W. Coughanour, "Phase equilibrium relations in the systems titania-niobia and zirconia-niobia." . J. Res. Natl. Bur. Stand., 55, 209 (1955).
- S. J. McCormack, K. Tseng, R. J. K. Weber, D. Kapush, S. V. Ushakov, A. Navrotsky, and W. M. Kriven, "In-situ determination of the HfO<sub>2</sub>-Ta<sub>2</sub>O<sub>5</sub>-temperature phase diagram up to 3000 °C." J. Am. Ceram. Soc., 102, 4848 (2019).
- P. P. Fedorov, "Comment on the paper: Scott J. McCormack, Kuo-Pin Tseng, Richard Weber et al 'In situ determination of the HfO<sub>2</sub> –Ta<sub>2</sub>O<sub>5</sub> -temperature phase diagram up to 3000 °C." J. Am. Ceram. Soc., 102, 7026 (2019).
- S. J. McCormack, K. Tseng, R. J. K. Weber, D. Kapush, S. V. Ushakov, A. Navrotsky, and W. M. Kriven, "Reply to comments: 'in-situ determination of the HfO<sub>2</sub>-Ta<sub>2</sub>O<sub>5</sub>-temperature phase diagram up to 3000 °C." *J. Am. Ceram. Soc.*, 102, 7028 (2019).
- S. J. McCormack, R. J. Weber, and W. M. Kriven, "In-situ investigation of Hf6Ta2O17 anisotropic thermal expansion and topotactic, peritectic transformation." Acta Mater., 161, 127 (2018).
- S. Jeon, "Composition-dependent structural integrity of Hf6Ta2O17 superstructure during sintering in a reducing atmosphere" Applied Sciences 10, 3871 (2020)
- during sintering in a reducing atmosphere." *Applied Sciences*, 10, 3871 (2020).
   Q. Liu, X. Hu, W. Zhu, J. Guo, and Z. Tan, "Effects of Ta<sub>2</sub>O<sub>5</sub> content on mechanical properties and high-temperature performance of Zr<sub>6</sub>Ta<sub>2</sub>O<sub>17</sub> thermal barrier coatings." *J. Am. Ceram. Soc.*, 104, 6533 (2021).
- J. Galy and R. S. Roth, "The crystal structure of Nb2Zr6O17." J. Solid State Chem., 7, 277 (1973).
- S. J. McCormack and W. M. Kriven, "Crystal structure solution for the A<sub>6</sub> B<sub>2</sub> O<sub>17</sub>
   (A = Zr, Hf; B = Nb, Ta) superstructure." Acta Crystallogr B Struct. Sci. Cryst.
   Eng. Mater., 75, 227 (2019).
- J. G. Thompson, R. L. Withers, J. Sellar, P. J. Barlow, and B. G. Hyde, "Incommensurate composite modulated Nb2Zrx-2O2x+1: X = 7.1-10.3." J. Solid State Chem., 88, 465 (1990).
- R. L. Withers, J. G. Thompson, and B. G. Hyde, "A modulation-wave approach to the structural description of the Nb<sub>2</sub>Zr<sub>x-2</sub>O<sub>2x+1</sub> (x = 7.1–10.3) solid-solution field." *Acta Crystallogr B Struct. Sci.*, 47, 166 (1991).
- D. Wiedemann, S. Orthmann, M. J. Mühlbauer, and M. Lerch, "Commensurate Nb<sub>2</sub>Zr<sub>5</sub>O<sub>15</sub>: accessible within the field Nb<sub>2</sub>Zr<sub>x</sub>O<sub>2x+5</sub> After All." *ChemistryOpen*, 8, 447 (2019).
- D. Wiedemann, T. Lüdtke, L. Palatinus, E. Willinger, M. G. Willinger, M. J. Mühlbauer, and M. Lerch, "At the gates: the tantalum-rich phase Hf<sub>3</sub> Ta<sub>2</sub> O<sub>11</sub> and its commensurately modulated structure." *Inorg. Chem.*, 57, 14435 (2018).

- A. A. Voskanyan, K. Lilova, S. J. McCormack, W. M. Kriven, and A. Navrotsky, "A new class of entropy stabilized oxides: commensurately modulated A6B2O17 (A = Zr, Hf; B = Nb, Ta) structures." Scr. Mater., 204, 114139 (2021).
- R. Jackson Spurling, C. Skidmore, N. S. McIlwaine, and J.-P. Maria, "Phase equilibria and metastability in the high-entropy A6B2O17 oxide family with A = Zr. Hf and B = Nb. Ta." *J. Mater. Sci.*, 58, 6164 (2023).
- 2Tr, Hf and B = Nb, Ta." J. Mater. Sci., 58, 6164 (2023).
  16. H. Li, Y. Yu, B. Fang, P. Xiao, W. Li, and S. Wang, "Calcium-magnesium-alumina-silicate (CMAS) corrosion behavior of A6B2O17 (A = Zr, Hf; B = Nb, Ta) as potential candidate for thermal barrier coating (TBC)." Corros. Sci., 204, 110395 (2022).
- S. Liu, X. P. Hu, Q. Liu, J. W. Guo, J. Y. Wu, and W. Zhu, "Effect of HfO2 content on CMAS corrosion resistance of a promising Hf6Ta2O17 ceramic for thermal barrier coatings." *Corros. Sci.*, 208, 110712 (2022).
- D. H. Triyoso, Z. Yu, R. Gregory, K. Moore, P. Fejes, and S. Schauer, "Thermal stability, microstructure, and electrical properties of atomic layer deposited Hf<sub>6</sub> Ta<sub>2</sub> O<sub>17</sub> gate dielectrics." *J. Mater. Res.*, 22, 2856 (2007).
- Q. Liu, X. P. Hu, W. Zhu, G. L. Liu, J. W. Guo, and J. Bin, "Thermal shock performance and failure behavior of Zr6Ta2O17-8YSZ double-ceramic-layer thermal barrier coatings prepared by atmospheric plasma spraying." *Ceram. Int.*, 48, 24402 (2022).
- J. Bai, Y. Huang, D. Wei, Z. Fan, and H. J. Seo, "Synthesis and characterization of semiconductor heterojunctions based on Zr6Nb2O17 nanoparticles." *Mater. Sci. Semicond. Process.*, 112, 105010 (2020).
   Y. Xue, Y. Cao, P. Ruan, M. Lu, F. Chen, W. Han, and W. Qiu, "A study of
- Y. Xue, Y. Cao, P. Ruan, M. Lu, F. Chen, W. Han, and W. Qiu, "A study of superstructure Hf<sub>6</sub> Ta<sub>2</sub> O<sub>17</sub> ceramics for electrochemical energy storage applications." Sustainable Energy Fuels, 7, 848 (2023).
- A. J. Moulson and J. M. Herbert, *Electroceramics: Materials, Properties*, Applications (Wiley, New York) 1st ed. (2003).
- B. M. Moshtaghioun, M. A. Laguna-Bercero, J. I. Peña, D. Gómez-García, and A. Domínguez-Rodríguez, "Cation-driven electrical conductivity in ta-doped orthorhombic zirconia ceramics." *Ceram. Int.*, 47, 7248 (2021).
- F. Cüppers, S. Menzel, C. Bengel, A. Hardtdegen, M. von Witzleben, U. Böttger, R. Waser, and S. Hoffmann-Eifert, "Exploiting the switching dynamics of HfO<sub>2</sub>-based ReRAM devices for reliable analog memristive behavior." APL Mater., 7, 091105 (2019).
- S. Privitera, G. Bersuker, S. Lombardo, C. Bongiorno, and D. C. Gilmer, "Conductive filament structure in HfO2 resistive switching memory devices." Solid-State Electronics, 111, 161 (2015).
- Ø. Johannesen and P. Kofstad, "Electrical conductivity of stabilized low and high temperature modifications of tantalum pentoxide." *Journal of the Less-Common Metals*, 98, 253 (1984).
- E. H. Greener, D. H. Whitmore, and M. E. Fine., "Electrical conductivity of nearstoichiometric a-Nb20 5t." The J. Chem. Phys., 34, 1017 (1961).
- P. Kofstad and D. J. Ruzicka, "On the defect structure of ZrO[Sub 2] and HfO[Sub 2]." J. Electrochem. Soc., 110, 181 (1963).
- M. Ali, G. Waltraud, M. KrivenMy, H. N. Gülgün, M. Ali, K. Waltraud, M. Nguyen, and M. Hoang, "Processes for preparing mixed metal oxide powders." U.S. Patent, 482, 387 (2002).
- M. H. Nguyen, S.-J. Lee, and W. M. Kriven, "Synthesis of oxide powders by way of a polymeric steric entrapment precursor route." J. Mater. Res., 14, 3417 (1999).
- D. A. G. Bruggeman, "Berechnung verschiedener physikalischer Konstanten von heterogenen Substanzen. I. Dielektrizitätskonstanten und Leitfähigkeiten der Mischkörper aus isotropen substanzen." Ann. Phys., 416, 636 (1935).
- H. Jiang, R. I. Gomez-Abal, P. Rinke, and M. Scheffler, "Electronic band structure of Zirconia and Hafnia polymorphs from the G W Perspective." *Phys. Rev. B*, 81, 085119 (2010).
- P. Kofstad, "Effect of impurities on the defects in oxides and their relationship to oxidation of metal." Corrosion, 24, 379 (1968).
- 34. J. W. Fergus, J. Mater. Sci., 38, 4259 (2003).
- M. Kim, S. Oh, B. Cho, and J. H. Joo, "Conduction mechanism in acceptor- or donor-doped ZrO<sub>2</sub> bulk and thin films." ACS Appl. Mater. Interfaces, 15, 31627 (2023).
- A. Kleger and V. Meunier, "Density functional theory study of the structural, electronic, mechanical, and thermal properties of Hf6Ta2O17." *Materials Today Communications*, 34, 105065 (2023).